AFRL-AFOSR-JP-TR-2016-0102

Study of solar energetic particles (SEPs) using largely separated spacecraft

Jinhye Park
KYUNG HEE UNIVERSITY, RESEARCH AND UNIVERSITY-INDUSTRY CORPORATION

10/29/2016
Final Report

Air Force Research Laboratory
AF Office Of Scientific Research (AFOSR)/ IOA
Arlington, Virginia 22203
Air Force Materiel Command

REPORT DOCUMENTATION PAGE

Form Approved
OMB No. 0704-0188

1. REPORT DATE *(DD-MM-YYYY)*	2. REPORT TYPE	3. DATES COVERED *(From - To)*
16-12-2016	Final	01 Sep 2013 to 31 Aug 2016

4. TITLE AND SUBTITLE
Study of solar energetic particles (SEPs) using largely separated spacecraft

5a. CONTRACT NUMBER

5b. GRANT NUMBER
FA2386-13-1-4066

5c. PROGRAM ELEMENT NUMBER
61102F

6. AUTHOR(S)
Jinhye Park

5d. PROJECT NUMBER

5e. TASK NUMBER

5f. WORK UNIT NUMBER

7. PERFORMING ORGANIZATION NAME(S) AND ADDRESS(ES)
KYUNG HEE UNIVERSITY, RESEARCH AND UNIVERSITY-INDUSTRY CORPORATION
KYUNG HEE UNIV, 1 SEOCHEON-DONG GIHEU
GYEONGGI-DO, 446-701 KR

8. PERFORMING ORGANIZATION REPORT NUMBER

9. SPONSORING/MONITORING AGENCY NAME(S) AND ADDRESS(ES)
AOARD
UNIT 45002
APO AP 96338-5002

10. SPONSOR/MONITOR'S ACRONYM(S)
AFRL/AFOSR IOA

11. SPONSOR/MONITOR'S REPORT NUMBER(S)
AFRL-AFOSR-JP-TR-2016-0102

12. DISTRIBUTION/AVAILABILITY STATEMENT
A DISTRIBUTION UNLIMITED: PB Public Release

13. SUPPLEMENTARY NOTES

14. ABSTRACT
Solar energetic particles (SEPs) are one of the main activities in terms of space weather forecast. SEPs could affect commercial airlines, HF communication, satellite launch, extra-vehicular activity from space stations, and manned space flight missions. In this study, we investigate the source regions and the characteristics of SEPs using multiple spacecraft data, Solar TErrestrial RElations Observatory Ahead (STEREO-A), Behind (STEREO-B) and Solar Dynamics Observatory (SDO)/Solar and Heliospheric Observatory (SOHO)/Geostationary Operational Environmental Satellites (GOES).

15. SUBJECT TERMS
solar wind, AOARD, solar physics, CME

16. SECURITY CLASSIFICATION OF:			17. LIMITATION OF ABSTRACT	18. NUMBER OF PAGES	19a. NAME OF RESPONSIBLE PERSON
a. REPORT	b. ABSTRACT	c. THIS PAGE			MAH, MISOON
Unclassified	Unclassified	Unclassified	SAR	23	19b. TELEPHONE NUMBER *(Include area code)* 042-511-2001

Standard Form 298 (Rev. 8/98)
Prescribed by ANSI Std. Z39.18

Study of solar energetic particles (SEPs) using largely separated spacecraft data

Abstract

Solar energetic particles (SEPs) are one of the main activities in terms of space weather forecast. SEPs could affect commercial airlines, HF communication, satellite launch, extra-vehicular activity from space stations, and manned space flight missions. In this study, we investigate the source regions and the characteristics of SEPs using multiple spacecraft data, Solar TErrestrial RElations Observatory Ahead (STEREO-A), Behind (STEREO-B) and Solar Dynamics Observatory (SDO)/Solar and Heliospheric Observatory (SOHO)/Geostationary Operational Environmental Satellites (GOES).

1. The source regions of solar energetic particles detected by widely separated spacecraft

The source regions of 12 solar energetic particle (SEP) events seen between 2010 August and 2012 January at STEREO-A, B, and/or Earth (Advanced Composition Explorer/Solar and Heliospheric Observatory/GOES), when the two STEREO spacecraft were separated by about 180◦. All events were asso- ciated with flares (C1 to X6) and fast coronal mass ejections and, except for one, accompanied by type II radio bursts. We have determined the arrival times of the SEPs at the three positions. Extreme ultraviolet (EUV) waves, observed in the 195 Å and 193 Å channels of STEREO and the Solar Dynamics Observatory, are tracked across the Sun to determine their arrival time at the photospheric source of open field lines connecting to the spacecraft. There is a good correlation between the EUV wave arrival times at the connecting footpoints and the SEP onset times. The delay time between electron onset and the EUV wave reaching the connecting footpoint is independent of distance from the flare site. The proton delay time increases with distance from the flare site. In three of the events, secondary flare sites may have also contributed to the wide longitudinal spread of SEPs.

1-1. Data and Analysis

To examine SEP fluxes, we use electron fluxes from the Solar Electron Proton Telescope (SEPT) on STEREO-A and STEREO-B averaged over 10 minute in 4 low energy channels (55 - 65 keV, 105 - 125 keV, 165 - 195 keV, and 295 – 335 keV) and 3 high energy channels (1 MeV, 2 MeV and 3.4 MeV) and from the AC Electron, Proton, and Alpha Monitor (EPAM) averaged over 5 min in 4 energy channels (38 - 53 keV, 53 -103 keV, 103 - 175 keV, and 175 - 315 keV). Proton fluxes are from the Low Energy Telescope (LET) averaged over 10 min in 3 energy channels (1.8 - 3.6 MeV, 4 - 6 MeV, and 6 - 10 MeV) and in 3 high energy channels (15 MeV, 25 MeV and 50 MeV) and from ACE EPAM averaged over 5 min at the 4 energy channels (0.31 - 0.58 MeV, 0.58 - 1.05 MeV, 1.05 - 1.89 MeV, and 1.89 - 4.75 MeV).

The interplanetary magnetic field emanates from the footpoints of coronal holes and streamers. Potential field source surface (PFSS) models give a good approximation of the magnetic field up to 2.5 R_{sun} and can be used to trace back the sources of the interplanetary field in the ecliptic plane at 2.5 R_{sun} (Neugebauer et al. 1998). Further out the field is stretched by the solar wind to form the Parker spiral, and so depends on the solar wind speed. The connection points of the spacecraft are obtained using synoptic magnetic field and ecliptic-plane PFSS extrapolations from the GONG website (http://gong.nso.edu/data/magmap/pfss.html). The gif images provided by the site have been rotated to Stonyhurst co-ordinates. The original connection points for Earth, STEREO-A and STEREO-B longitudes shown on the plots do not account for the Parker spiral. Therefore we move the connection points at 2.5 Rsun, westward according to the solar wind speed observed at the time of the events using the equation, $Ø_0 = D_Ω/Vw + Ø$ where Ø, $Ø_0$ are the spacecraft and solar longitudes, D is the distance to the Sun, Vw is the solar wind speed, and Ω is the solar rotation rate.

The Stonyhurst heliographic (Earth-view) image combined two STEREO 195 Å image with the nearest in time SDO/AIA 193 Å provides full Sun view. We identify the source regions related to SEPs using the Stonyhurst heliographic movie. Also, we can get a ratio image of the Sun at the time of

the EUV wave showing the positions of space-time cuts in the direction of the footpoints of the connecting open field line to each spacecraft as well as space-time running ratio images along those cuts. We can determine the EUV wave properties using the ratio images (Figure 1).

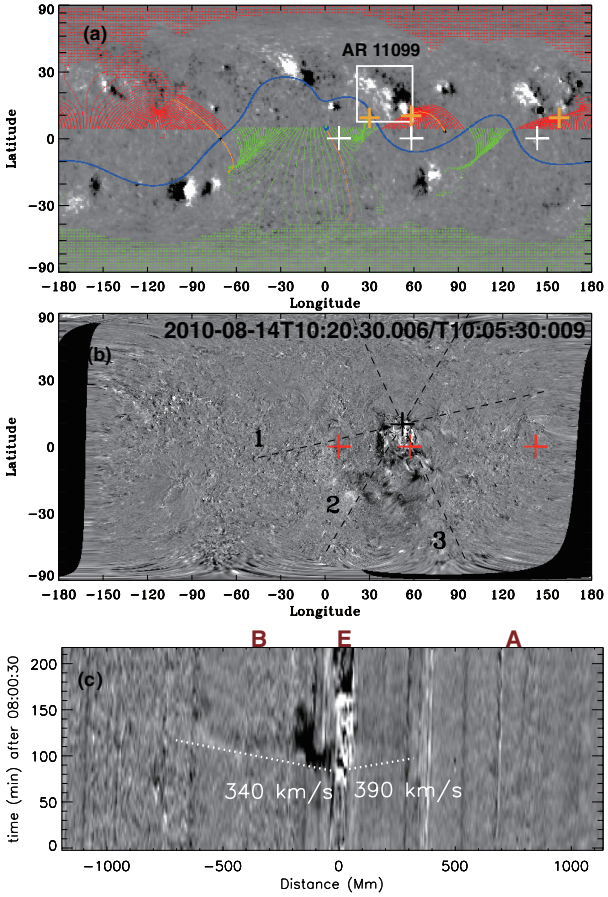

Figure 1. 2010 August 14 source region and EUV wave: (a) GONG synoptic magnetic field with PFSS ecliptic plane field lines traced back to their source. White and red crosses mark the longitudes of STB, Earth, and STA at 2.5R⊙. The photospheric footpoints of the connecting field lines are marked by orange crosses. Connecting footpoints are deduced by tracing the field lines from the white crosses to the Sun. Green/red indicates positive/negative open fields. The source region is enclosed by a white square. (b) Full Sun ratio image at the times given. This is a composite of STB 195 Å, SDO 193 Å, and STA 194 Å images. The dashed line indicates the position of the space–time image below. (c) Running ratio space–time image along the line in (b). The white number is the approximate wave speed calculated by manually choosing the start and end positions of the wave.

Table 1 lists the 12 SEP events and their associated solar phenomena. The events are related to flares ranging from C1 to X6 in X-ray strength and fast CMEs ranging from 1005 km/s to 2256 km/s with an average speed of 1470 km/s. All are accompanied by a type III radio burst and all but one are accompanied by a type II radio burst. The underlined event appears to have been caused by flares in more than one AR, although there was only one EUV wave, CME, and type II burst. The average EUV wave speeds, computed from the space–time images, are given in the table.

Table 1. The Solar Sources of the 12 SEP Events.

Event	Date	Flare[a] Start	Max	Class	Location	AR	CME[b] Time	V(km s^{-1})	Radio[c] II Time	Radio[d] III Time	EUV[e] V(km s^{-1})
1	20100814	09:38	10:05	C4.4	N17W52	11099	$10:12^{L}$	1205^{L}	10:00	09:55	310
2	20100818	04:45	05:48	C4.5	N17W91	11099	$05:24^{A}$	1250^{A}	06:05	05:30	200
3	20110307	19:43	20:12	M3.7	N24W59	11164	$20:00^{L}$	2256^{L}	20:00	19:50	510
4	20110321	02:04	...	...	N22W132	...	$02:24^{B}$	1562^{B}	02:20	02:20	528
5	20110804	03:41	03:57	M9.3	N15W49	11261	$03:54^{A}$	1785^{A}	04:15	03:50	510
6	20110809	07:48	08:05	X6.9	N17W83	11263	$08:12^{L}$	1610^{L}	08:20	08:00	420
7	20110921	21:35[f]	...	...	N15W120	...	$22:12^{L}$	1007^{L}	...	21:40?	225
8	20110922	10:28	11:01	X1.4	N11E74	11302	$10:48^{L}$	1905^{L}	11:05	10:40	760
9	20111103	21:40	...	...	N05E160	...	$22:54^{A}$	1136^{A}	22:35	22:15	473
		22:28	22:35	C5.8	N18E60	11339	...	...	...	...	...
		22:12	22:18	C5.4	N10W85	11333	...	...	...	...	...
10	20111126	06:40	07:10	C1.2	N08W49	11353	$07:12^{B}$	1005^{B}	07:15	07:10	380
11	20120123	03:38	03:59	M8.7	N28W36	11402	$03:54^{B}$	1785^{B}	04:00	03:40	525
12	20120127	17:37	18:37	X1.7	N27W71	11402	$18:27^{L}$	1136^{L}	18:30	18:15	715

Notes. The underlined events are likely related to multiple source regions.
[a] Flare times are taken from ftp://ftp.ngdc.noaa.gov/STP/space-weather/solar-data/solar-features/solar-flares/x-rays/goes.
[b] CME time is the appearance in LASCO C2 or SECCHI COR2 field of view. CME times are taken from http://cdaw.gsfc.nasa.gov/CME_list and http://secchi.nrl.navy.mil/cactus. L is *SOHO*/LASCO. A and B are *STA*/COR2 and *STB*/COR2, respectively.
[c] Radio II times are taken from http://ssed.gsfc.nasa.gov/waves/data_products.html except for 20100814, which was taken from http://secchirh.obspm.fr.
[d] Radio III times are taken from http://secchirh.obspm.fr.
[e] EUV wave speeds are the average speeds from the source to the spacecraft connecting points.
[f] The brightening was observed around the west limb at 21:35 UT on 2011 September 21.

1-2. Result

From this study, we have found that nine events were related to a single source region and the other three were probably due to multiple sources. Five events had strong flux enhancements in all three spacecraft. Eruptions from multiple source regions sometimes cause abrupt flux enhancements simultaneously at widely separated positions. The most notable event was likely the one on 2011 November 3 that showed abrupt enhancements at *STB*, Earth, and *STA*. There may have been three different sources that erupted at almost the same time and were connected to *STB*, Earth, and *STA* but one needs to look at coronagraph data to identify the SEP sources. This will be done in a follow-up analysis. Another unusual event possibly related to multiple sources was the event on 2011 November 26. First, a large trans-equatorial filament erupted with good connection to Earth. Later, neighboring ARs produced a jet and small flare connected to STB and STA, respectively. In particular, the source region was the biggest in our study and the solar activities associated with the event had a long duration (~100 minutes). In all the SEP events, EUV waves (average speed ~463 km/s) were observed with fast CMEs (average speed ~1470 km/s).

To examine the relationship between EUV waves and the sites of SEP acceleration, we have considered an offset time using flare, CME, and type III radio burst times against which we can compare the SEP onset and EUV arrival times. SEP onset times are significantly associated with EUV wave arrival times. Our result shows that the correlation coefficients between the two parameters are between 0.60 and 0.69 (Figures 2-3). The results support the idea that EUV waves trace the release sites of SEPs, which is consistent with previous studies that suggested that SEPs are accelerated by large coronal shock waves (Kocharov et al. 1994; Torsti et al. 1998; Krucker et al. 1999; Vainio & Khan 2004; Rouillard et al. 2012).

In this study, most events were associated with complex solar sources and flux enhancements. Although direct open magnetic field connections play an important role in generating SEP events with strong flux enhancements, in our study, the flux enhancements were observed in 19 electron cases and 14 proton cases without magnetic field connections. Kozarev et al. (2011) found that protons that came from a site with an open field geometry were quickly accelerated into interplanetary space, while protons associated with a closed field geometry were probably accelerated in shocks. The fact that all strong events reported in our study were associated with type II radio emission supports the idea that the SEP events were generated by CME- driven shocks. The observations of the flux enhancements show that the shocks can spread over at least ~180°.

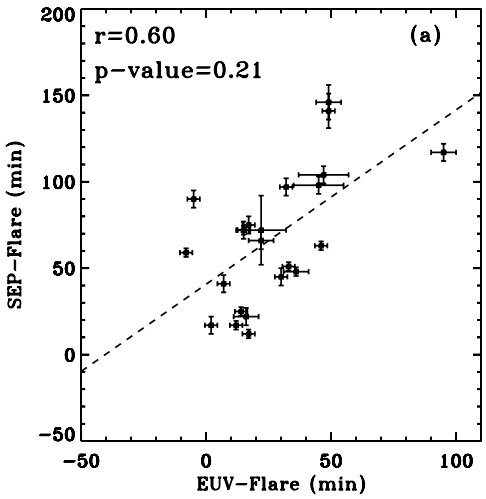

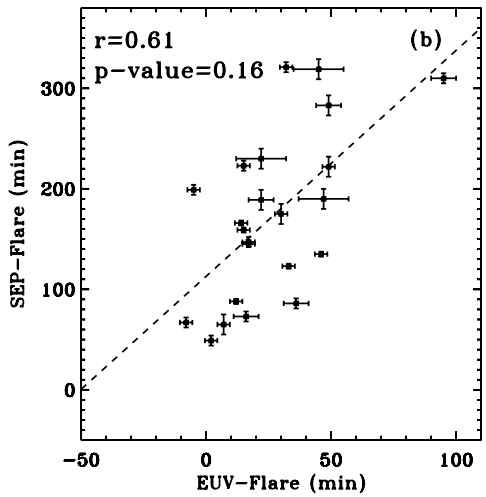

Figure 2. Relationship between EUV flare time and SEP flare time: (a) electron and (b) proton. The error bars represents the number of degradations. The dashed line is a linear least squares fit to the data. In the figure, r means a correlation coefficient and the p-value is the probability that r = 0.

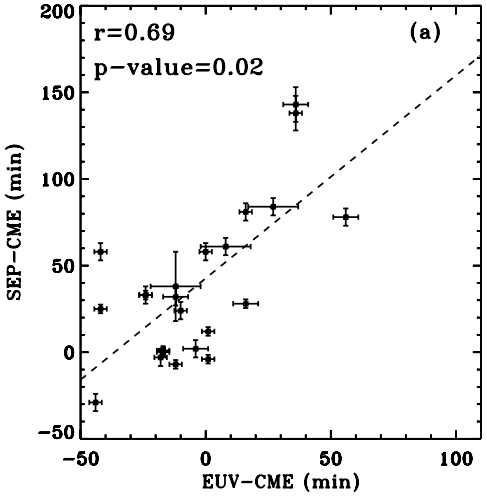

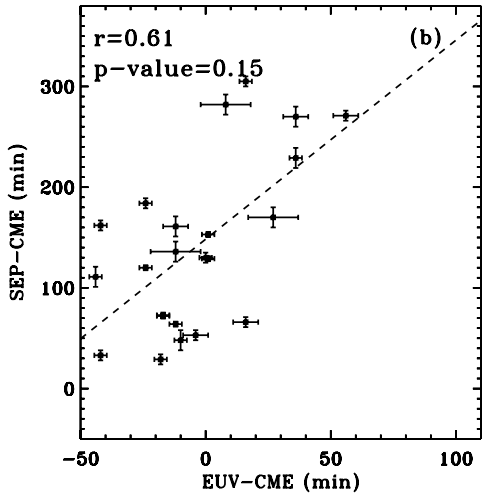

Figure 3. Relationship between EUV-CME time and SEP-CME time: (a) electron and (b) proton. The error bars represents the number of degradations. The dashed line is a linear least squares fit to the data. In the figure, r means a correlation coefficient and the p-value is the probability that r = 0.

2. What flare and CME parameters control the occurrence of solar proton events? (Park et al. 2014, JGR)

In this study we examine the occurrence probabilities of solar proton events (SPEs) and their 12 peak fluxes depending on both flare and coronal mass ejection (CME) parameters: flare peak flux, longitude, 13 impulsive time, CME linear speed, and angular width. For this we use the NOAA SPEs, their associated X-ray 14 flares, and CME from 1997 to 2011. We divide the data into 16 subgroups according to the flare and CME 15 parameters and estimate the SPE probabilities for the subgroups. The three highest probabilities are found 16 for the following subgroups: (1) fast full halo (55.3%) and fast partial halo (42.9%) CMEs associated with 17 strong flares from the western region and (2) slow full halo CMEs associated with strong flares from the 18 western region (31.6%). It is noted that the events whose SPE probabilities are nearly 0% belong to the 19 following subgroups: (1) slow and fast partial halo CMEs from the eastern region, (2) slow partial halo CMEs 20 from the western region, and (3) slow full halo CMEs from the eastern region. These results show that 21 important parameters to control SPE occurrences are CME linear speed, angular width, and source 22 longitude, which can be understood by the piston-driven shock formation of fast CMEs and magnetic field 23 connectivity from the source site to the Earth. It is also shown that when the subgroups are separately 24 considered by flare impulsive time and source longitude, the correlation coefficients between the observed 25 and the predicted SPE peak fluxes are greatly improved.

2-1. Data and Analysis

We use the NOAA SPE list (http://swpc.noaa.gov/ftpdir/indices/SPE.txt) from 1997 to 2011 and the information of their related CMEs observed by the Solar and Heliospheric Observatory mission (SOHO) Large Angle and Spectrometric Coronagraph (LASCO) [*Brueckner et al.*, 1995]. The projected CME linear speeds and angular widths are taken from the SOHO LASCO CME online catalog (http://cdaw.gsfc.nasa.gov/ CME_list/) [*Gopalswamy et al.*, 2009]. Flare information is taken from the NOAA National Geophysical Data Center (NGDC) Geostationary Operational Environmental Satellite (GOES) X-ray flare catalog (http://www. ngdc.noaa.gov/ngdc.html).

To examine SPE occurrence probabilities, we consider four solar eruption parameters: flare peak flux, source longitude, CME linear speed, and angular width. The previous studies [Park et al., 2010, 2012] showed that it is extremely rare that SPEs are generated by narrow (< 120°) and slow (< 400 km/s) CMEs as well as weak flares (< C1 class). We exclude the events generated by relatively weak solar eruptions, which are only two from 1996 to 2011, and do not consider events whose source regions are behind the limb. Accordingly, we use 67 SPEs and 490 solar eruptions, which meet the criteria of the parameters as follows: flare peak flux ≥ C1 class, CMEs linear speed ≥ 400 km/s, angular width ≥ 120◦, and front source longitude ($-90° \le L \le 90°$).

For the regression between solar eruption parameters and SPE peak flux, we use five solar eruption parameters associated with the observed SPEs. The parameters are flare peak flux, source longitude, impulsive time, CME linear speed, and angular width. In this case, we exclude two events because the events have unusual long impulsive times (2.66 h and 1.76 h) which are significantly larger than 1.39, mean (0.55) plus 2 times standard deviation (0.42). For the regression, we use 65 SPEs and their associated eruptions.

2-2 Result

Our results have shown that the SPE occurrence probabilities are strongly dependent on flare and CME parameters and the distinct contrasts of the probabilities are seen according to the quantitative ranges of the parameters (Tables 2 and 3). The highest probabilities have been found in the subgroups of fast full halo CMEs (55.3%) and partial halo CMEs (42.9%) associated with strong flares from the western region. The probability is also high for the subgroup of slow full halo CMEs associated with strong flares from the western region (31.6%). Noticeably, the SPE probabilities are nearly 0% for eight subgroups. As shown in Table 2, slow full halo CMEs from the eastern region have no SPE. As for the partial halo CMEs in Table 3, all eastern events have no SPE and western slow CMEs have only one SPE. These results show that CME linear speed, angular width, and source longitude are the most important parameters to control SPE occurrences. This is understood by that wide and fast CMEs can form piston-driven shocks, which is the main mechanism to accelerate SPEs. The importance of source longitude and angular width can be interpreted by the sub-Earth point, which is directly linked to the Earth by the Parker spiral magnetic fields. Our results are the same line with *Kahler and Reames* (2003) and *Gopalswamy et al.* (2008). *Kahler and Reames* (2003) found that CMEs having w ide angular widths are mostly fast ($V \geq 900 \mathrm{kms}^{-1}$) and associated with SPEs. They noted that CMEs with narrow angular widths are unsuitable to form CME-driven shocks accelerating SPEs. *Gopalswamy et al.* (2008) also showed that the SPE occurrences increase with CME linear speeds and angular widths. They found that some CMEs with DH type II bursts as coronal shock signatures are not associated with SPEs, mainly because of poor connectivity or it is possible that the shocks with the bursts are too weak to accelerate SPEs (*Shen et al.*, 2007).

Table 2. SPE Occurrence Probability Depending on Flare Peak Flux, Longitude, and CME Linear Speed (Slow CME: 400 km/s ≤ V < 1000 km/s and Fast CME: $V \geq$ 1000 km/s) for Full Halo CMEs

Location	Flare		Slow CME	Fast CME	Total
West	$f \geq$ M5	P	31.6%	55.3%	47.4%
		σ	10.7%	8.1%	6.6%
		N	6/19	21/38	27/57
West	$f <$ M5	P	13.2%	28.6%	20.5%
		σ	5.5%	7.6%	4.7%
		N	5/38	10/35	15/73
East	$f \geq$ M5	P	0%	29.6%	22.9%
		σ	0%	8.8%	7.1%
		N	0/8	8/27	8/35
East	$f <$ M5	P	0%	21.7%	7.9%
		σ	0%	8.6%	3.4%
		N	0/40	5/23	5/63
Total		P	10.5%	35.5%	24.1%
		σ	3.0%	4.3%	2.8%
		N	11/105	44/123	55/228

[a] P refers to the probability and σ is the uncertainty of the probability and is calculated by $\sigma=\sqrt{\frac{p(1-p)}{n}}$, where n is the number of solar eruptions. N is the ratio of SPEs to solar eruptions.

Table 3. SPE Occurrence Probability Depending on Flare Peak Flux, Longitude, and CME Linear Speed (Slow CME: 400 km/s ≤ V < 1000 km/s and Fast CME: $V \geq 1000$ km/s) for Partial Halo CMEs.

Location	Flare		Slow CME	Fast CME	Total
West	$f \geq$ M5	P	0%	42.9%	22.2%
		σ	0%	13.2%	8.0%
		N	0/13	6/14	6/27
West	$f <$ M5	P	1.2%	17.9%	5.5%
		σ	1.2%	7.2%	2.2%
		N	1/81	5/28	6/109
East	$f \geq$ M5	P	0%	0%	0%
		σ	0%	0%	0%
		N	0/2	0/11	0/13
East	$f <$ M5	P	0%	0%	0%
		σ	0%	0%	0%
		N	0/90	0/23	0/113
Total		P	0.5%	14.5%	4.6%
		σ	0.5%	4.0%	1.3%
		N	1/186	11/76	12/262

[a] P refers to the probability and σ is the uncertainty of the probability and is calculated by $\sigma=\sqrt{\frac{p(1-p)}{n}}$, where n is the number of solar eruptions. N is the ratio of SPEs to solar eruptions.

Table 4. The Results of Multiple Regressions of SPE Peak Fluxes and Associated Solar Eruption Parameters for 20 Subgroups as in Table 3.

Criteria	N	a	b	r	p	a_0	a_1	a_2	a_3	a_4	a_5	N_p	Figure
$T <$ 0.4 h	28	0.35	1.42	0.59	<0.001	1.07	0.20	0.84×10^{-3}	−0.50	-0.11×10^{-1}	0.74×10^{-3}	5	3a
$T \geq$ 0.4 h	37	0.61	0.92	0.78	<0.001	0.06	0.42	0.78×10^{-3}	1.58	0.43×10^{-2}	-0.14×10^{-2}	5	3b
$T \geq$ 0.4 h/east	12	0.90	0.24	0.95	<0.001	0.28	0.19	0.42×10^{-3}	2.36	0.13×10^{-1}	—	4	3c
$T \geq$ 0.4 h/west	25	0.54	1.08	0.73	<0.001	0.59	0.41	0.89×10^{-3}	1.22	-0.88×10^{-3}	-0.20×10^{-2}	5	3d
East	13	0.90	0.22	0.95	<0.001	0.28	0.19	0.42×10^{-3}	2.36	0.13×10^{-1}	—	4	–
West	52	0.41	1.36	0.64	<0.001	1.41	0.37	0.71×10^{-3}	0.89	-0.97×10^{-2}	-0.14×10^{-2}	5	–
West/$T <$ 0.4 h	27	0.43	1.26	0.66	<0.001	1.34	0.17	0.88×10^{-3}	−0.17	-0.16×10^{-1}	0.37×10^{-3}	5	–
West/$T \geq$ 0.4 h	25	0.54	1.08	0.73	<0.001	0.59	0.41	0.89×10^{-3}	1.22	-0.88×10^{-3}	-0.20×10^{-2}	5	–
$F <$ M5	25	0.27	1.33	0.52	0.006	0.64	−0.58	0.86×10^{-3}	0.21×10^{-1}	0.24×10^{-3}	0.26×10^{-3}	5	–
$F \geq$ M5	40	0.40	1.54	0.63	<0.001	1.22	0.43	0.39×10^{-3}	1.27	0.81×10^{-3}	-0.15×10^{-2}	5	–
$F \geq$ M5/$T <$ 0.4 h	22	0.40	1.34	0.63	0.001	2.30	0.43	0.75×10^{-3}	−0.11	-0.13×10^{-1}	-0.35×10^{-2}	5	–
$F \geq$ M5/$T \geq$ 0.4 h	18	0.54	1.37	0.73	<0.001	0.13	0.59	0.45×10^{-3}	1.50	0.65×10^{-2}	0.52×10^{-6}	5	–
AW< 360°	12	0.83	0.40	0.91	<0.001	−1.37	0.29	0.28×10^{-3}	2.00	0.31×10^{-1}	0.36×10^{-3}	5	–
AW = 360°	53	0.33	1.51	0.58	<0.001	0.58	0.38	0.60×10^{-3}	0.81	0.12×10^{-2}	—	4	–
AW = 360°/$T <$ 0.4 h	24	0.36	1.41	0.60	0.002	1.37	-0.12×10^{-2}	0.10×10^{-2}	−0.81	-0.12×10^{-1}	—	4	–
AW = 360°/$T \geq$ 0.4 h	29	0.57	0.98	0.76	<0.001	−0.28	0.42	0.68×10^{-3}	1.63	0.35×10^{-2}	—	4	–
$V <$ 1000 km s^{-1}	11	0.48	0.77	0.69	0.016	2.28	−0.58	-0.27×10^{-2}	−1.07	-0.91×10^{-2}	0.79×10^{-2}	5	–
$V \geq$ 1000 km s^{-1}	54	0.32	1.66	0.57	<0.001	0.80	0.47	0.35×10^{-3}	1.19	0.20×10^{-2}	-0.18×10^{-3}	5	–
$V \geq$ 1000 km s^{-1}/east	13	0.90	0.22	0.95	<0.001	0.28	0.19	0.42×10^{-3}	2.36	0.13×10^{-1}	—	4	–
$V \geq$ 1000 km s^{-1}/west	41	0.38	1.56	0.61	<0.001	1.93	0.45	0.40×10^{-3}	1.26	-0.13×10^{-1}	-0.14×10^{-2}	5	–

[a] N is the number of SPEs used for the regressions. N_p represents the number of parameters used for the regressions. In the case of N_p = 5, we use the five parameters, flare peak flux (F), impulsive time (T), longitude, CME linear speed (V), and angular width (AW). The AW is excluded in the case of N_p = 4. The regressions are based on forecasted values derived from the observed parameters.

We present the relationships between the observed and the predicted SPE peak fluxes using the multiple regression method combining the solar eruption parameters (flare peak flux, longitude, impulsive time, CME linear speed, and angular width) for 20 subgroups whose criteria are given in Table 4. In case that all of the events are associated with full halo CMEs, we only consider four parameters except for the angular width.

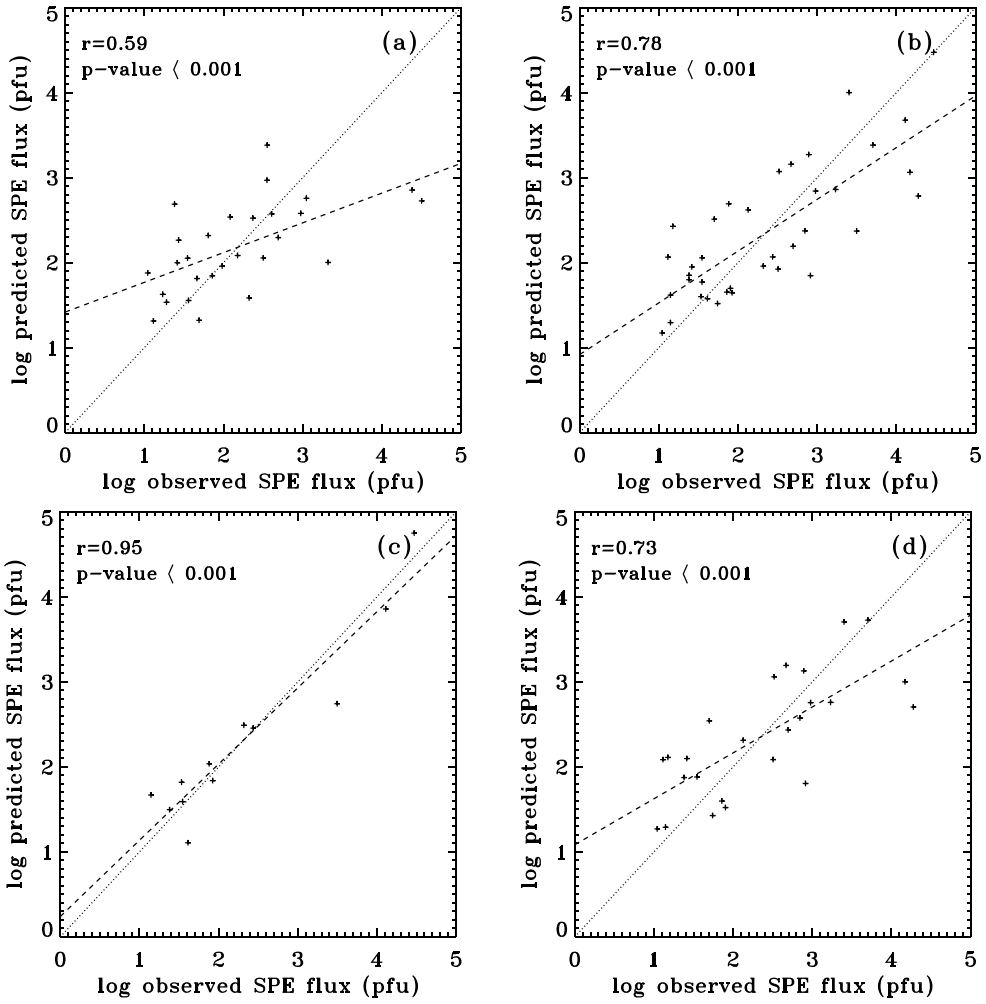

Figure 4. Relationship between the observed and the predicted SPE peak fluxes which are estimated by the multiple regression method using the five parameters of the solar eruptions (flare peak flux, impulsive time, longitude, CME linear speed, and angular width) according to the criteria: (a) the subgroup of impulsive time < 0.4 h, (b) the subgroup of impulsive time ≥ 0.4 h, (c) the subgroup of impulsive time ≥ 0.4 h and the eastern region, and (d) the subgroup of impulsive time ≥ 0.4 h and the western region. The dashed lines represent the least squares fittings from multiple regressions. The coefficients of the fittings are given in the Table 4.

When we take into account the impulsive times, short duration ($T < 0.4$ h) and long duration ($T \geq 0.4$ h), the correlation coefficients between the observed and the predicted SPE peak fluxes are 0.59 for the short-duration case (Figure 4a) and 0.78 for the long-duration case (Figure 4b). For the long-duration case, the correlation coefficients are 0.95 for the eastern events (Figure 4c) and 0.73 for the western events (Figure 4d). Noticeably, the coefficient for the eastern long-duration events is significantly high. The slope of the linear fitting (0.90) is close to 1.0.

3. Study of solar energetic particle associated with coronal EUV waves (Park et al., 2015, ApJ)

We study the relationship between large gradual solar energetic particle (SEP) events and associated extreme ultraviolet (EUV) wave properties in 16 events that occurred between 2010 August and 2013 May and were observed by STEREO, SOHO or SDO. We determine onset times, peak times and peak fluxes of the SEP events in SOHO ERNE and STEREO LET proton channel (6-10 MeV). The EUV wave arrival times and their speeds from the source sites to the spacecraft footpoints in the photosphere, which are magnetically connected to the spacecraft by Parker spiral potential fields, are determined by space-time plots from the full Sun heliographic images created by combining STEREO-A, B 195 ˚A and SDO 193 ˚A images. It is noted that there is a significant correlation between the EUV wave arrival times and the proton onset times (r=0.73) but not the proton peak times. The SEP peak fluxes increase with the EUV wave speeds (r=0.69) and the SEP spectral indices become harder with the speeds. The present study shows that higher energetic particle fluxes are strongly associated with faster EUV waves, which are considered as the lateral expansions of CME-driven shocks in the low corona.

3-1. Data and Analysis

For the study, we consider the 28 events detected by the Low Energy Telescope (LET; Mewaldt et al. 2008) on STEREO averaged over 10 minutes in the 6–10 MeV proton channel or by the Energetic and Relativistic Nuclei and Electron instrument (ERNE; Torsti et al. 1995) on SOHO averaged over 10 minutes in the 6–10 MeV proton channel from 2010 August to 2013 May. Among the events, we do not consider proton enhancements affected by solar activities outside the main eruptions, thus avoiding any complex flux profiles. In addition, we disregard events where strong active regions (ARs) are located in the paths of EUV wave propagation toward the spacecraft magnetic footpoints because the EUV waves can be refracted and reflected by the ARs, or attenuated though the ARs. Finally, we get 16 events for the period, which are given in Table 5. The solar sites are determined by identifying eruptions in full-Sun EUV Stonyhurst heliographic images composed of the two STEREO Extreme-Ultraviolet Imager (EUVI; Wuelser et al. 2004) 195 Å images and SDO/AIA 193 Å images with a cadence of 5 minutes. We also use the GOES flare list (http:// solar-center.stanford.edu/SID/activities/PickFlare.html), the SOHO LASCO CME catalog (http://cdaw.gsfc.nasa.gov/CME_list), the CACTus COR2 CME list (http://sidc.oma.be/cactus), and the type II radio burst lists compiled by the Wind and STEREO data center (http://ssed.gsfc.nasa.gov/waves/data_products.html).

Table 5. The Solar Sources of the SEP Events.

	Flare[b]					CME[c]		
Date	Start	Max	Class	Location	AR	Time	V_c(km s^{-1})	Type II[d]
2010 Aug 14[a]	09:38	10:05	C4.4	N17W52	11099	10:12^{L}	1205^{L}	10:00
2010 Aug 18[a]	04:45	05:48	C4.5	N17W91	11099	05:24^{A}	1250^{A}	06:05
2011 Mar 7[a]	19:43	20:12	M3.7	N24W59	11164	20:00^{L}	2256^{L}	20:00
2011 Mar 21[a]	…	…	…	N22W132	…	02:24^{B}	1562^{B}	02:30
2011 Aug 4[a]	03:41	03:57	M9.3	N15W49	11261	03:54^{A}	1785^{A}	04:15
2011 Sep 21[a]	…	…	…	N15W120	…	22:12^{L}	1007^{L}	…
2011 Sep 22[a]	10:28	11:01	X1.4	N11E74	11302	10:48^{L}	1905^{L}	11:05
2011 Nov 3[a]	…	…	…	N05E160	…	22:54^{A}	1136^{A}	22:35
2012 Jan 23[a]	03:38	03:59	M8.7	N28W36	11402	03:54^{B}	1785^{B}	04:00
2012 May 26	…	…	…	N15W120	11482	20:57^{L}	1966^{L}	20:50
2012 Jul 18	…	…	…	N15W170	…	06:24^{B}	1041^{B}	06:15
2012 Jul 23	…	…	…	S17W135	…	02:36^{L}	2003^{L}	02:30
2012 Aug 31	19:45	20:43	C8.4	S19E42	11564	20:12^{L}	1442^{L}	20:00
2013 Mar 15	05:46	06:58	M1.1	N11E12	11692	07:12^{B}	1136^{B}	07:00
2013 Apr 11	06:55	07:16	M6.5	N09E12	11719	07:24^{B}	1388^{B}	07:10
2013 May 13	01:53	02:17	X1.7	N08E89	11748	02:12^{L}	1302^{L}	02:20

Notes. SEP fluxes were measured by the *SOHO*/ERNE 5.95–10.1 MeV channel or the *STEREO*/LET 6–10 MeV channel over 10 minutes.
[a] Events were investigated in Park et al. (2013).
[b] Flare information is taken from ftp://ftp.ngdc.noaa.gov/STP/space-weather/solar-data/solar-features/solar-flares/x-rays/goes.
[c] CME information is taken from http://cdaw.gsfc.nasa.gov/CME_list and http://secchi.nrl.navy.mil/cactus. The CME time is the first appearance time in the LASCO C2 or SECCHI COR2 field of view. L is *SOHO*/LASCO. A and B are *STEREO-A*/COR2 and *STEREO-B*/COR2, respectively.
[d] Radio type II times are taken from http://ssed.gsfc.nasa.gov/waves/data_products.html.

3-2. Result

We found that the 6–10 MeV SEP peak fluxes increase with the EUV wave speeds measured along the direction from the source regions to the footpoints of the spacecraft. It is also seen that the proton spectral indices measured at higher energies become harder with the EUV wave speeds. These results imply that faster waves are related to the acceleration of SEPs of higher fluxes and energies and suggest that EUV wave speeds represent the strengths of the lateral coronal disturbances in CME-driven shocks (Figure 5).

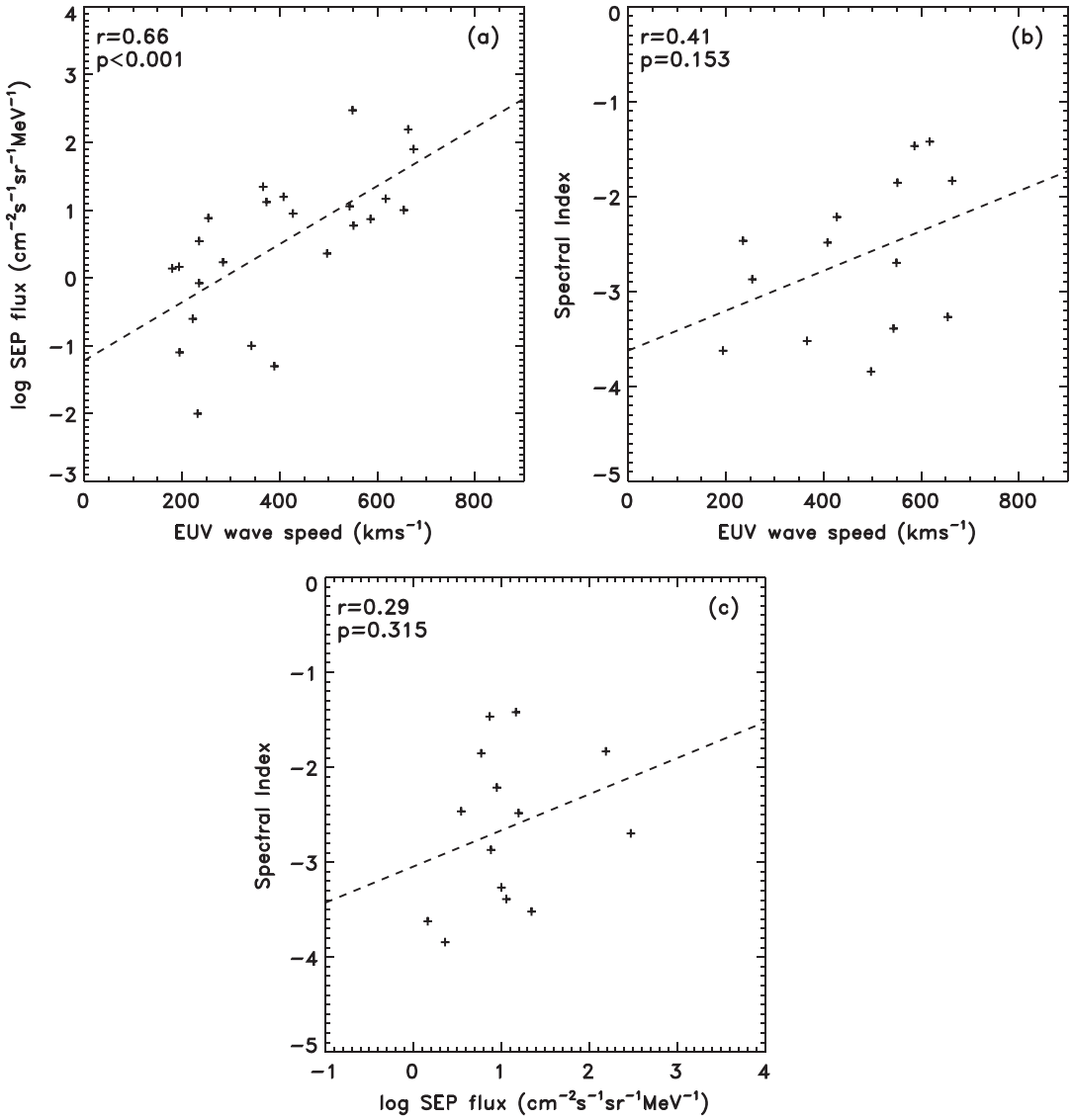

Figure 5. Relationships between SEPs and the EUV waves: (a) 6–10 MeV proton peak fluxes vs. wave speeds for 24 cases, (b) two-point power-law spectral indices vs. wave speeds for 14 cases, and (c) 6–10 MeV proton peak fluxes vs. two-point power-law spectral indices. The spectral indices of SEP events were obtained at the proton peak fluxes in the SOHO/ERNE 20.8–26.0 MeV and 34.8–40.5 MeV and STEREO/HET 20.8–23.8 MeV and 35.5–40.5 MeV channels. The dashed lines are linear least-squares fits to the data. In each figure, r is the correlation coefficient and p is the p-value.

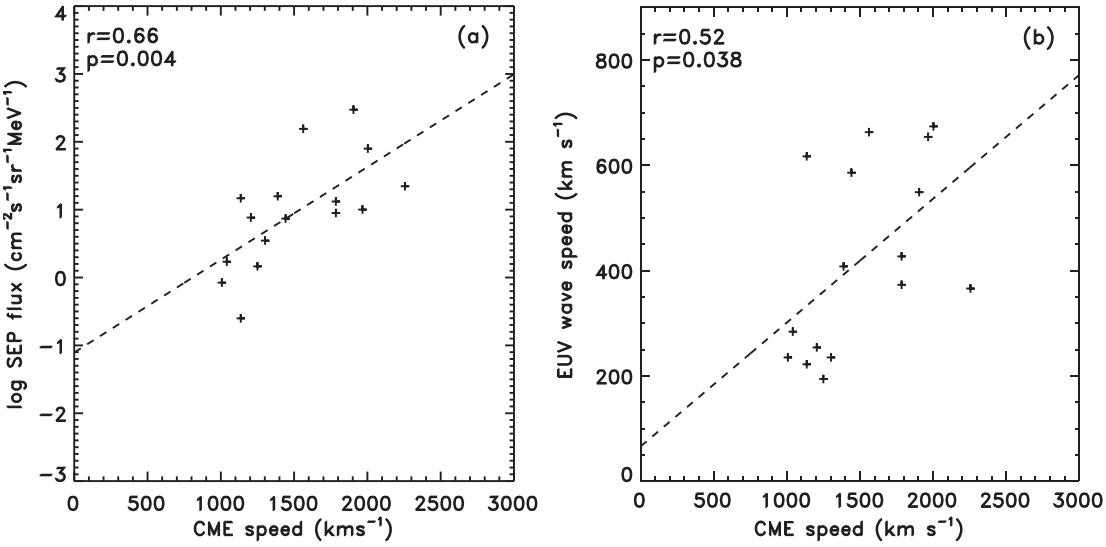

Figure 6. Relationship between SEPs, EUV waves, and CME linear speeds for 16 events: (a) CME linear speed vs. 6–10 MeV proton peak flux, and (b) CME linear speed vs. EUV wave speed. The dashed line is a linear least-squares fit to the data. In the figure, r is the correlation coefficient and p is the p-value.

In Figure 6a we show the relationship between the CME linear speeds and the SEP peak fluxes for the 16 events in Table 2. If SEP events were observed by more than two instruments, we selected the highest flux among them. The correlation coefficient is 0.66 ± 0.20, which is similar to ones found in previous studies (Park et al. 2012; Kahler & Vourlidas 2014). In the case of EUV wave speeds using the same data set, the correlation coefficient is 0.75. The results show that both the CME speeds and the EUV wave speeds are associated with SEP peak fluxes. Figure 6b shows the relationship between CME speeds and EUV wave speeds for the 16 events. The correlation coefficient (r = 0.52 ± 0.23) is meaningful even though the direct comparison of EUV and CME characteristics is difficult because it is not easy to trace CME speeds in the high coronal region along the directions of the EUV wave propagations in the low coronal region.

4. Characteristics of solar energetic protons in solar cycle 24 using stereoscopic observation (In preparation)

In the present study, we examine the characteristics of 18 solar energetic particles (SEPs) on 3 dimensional (3D) CME parameters (radial speed and angular width) using 40 measurements of multiple spacecraft (SOHO, STEREO-A and B). To obtain 3D CME parameters, we reconstruct CMEs used by STEREO CME Analysis Tool (StereoCAT) from 2010 August to 2013 June. Longitudinal angular separations (θ_S) between SEP source regions and magnetic footpoints of the spacecraft are also considered. The main results are as follows. 1) We find that the dependence of SEPs on 3D CME speed are similar to that of 2 dimensional (2D) CME speed. 2) There is a weak tendency that the SEP peak flux increases with 3D angular width, while the 2D angular widths of all CMEs except for three events are 360°. 3) There is a noticeable anti-correlation (r=-0.62) between SEP peak flux and angular separation for 40 measurements. 4) All 17 measurements whose magnetic footpoints are located inside the CME angular widths, have SEP enhancements but about 40% of the measurements (14/37) whose footpoints are located outside, have no SEP enhancement. 5) Multiple spacecraft observations show that most strong SEP events are associated with very fast CMEs whose angular separations are closer to zero within the 3D angular widths.

4-1 Data and Analysis

For the present study, we search 38 strong SEPs from 2010 to 2015 based on NOAA list. Among them, we exclude the events whose proton flux profile are unclear and complicated due to multiple solar activities as well as the events whose 3D CME parameters cannot be obtained due to data gap. As a result, we select 18 events (Table 6) that are possible to study the relationship between SEPs and 3D CME parameters. They are mostly associated with the events in NOAA solar proton event list except two events (2010 August 18 and 2011 September 21).

We take the proton peak fluxes of 8 events from Park et al. (2015), which are obtained from twin STEREO/Low Energy Telescope (LET: Mewaldt et al. 2008) and SOHO/Energetic and Relativistic Nuclei and Electron instrument (ERNE: Torsti et al. 1995) averaged over 10 min in 6-10 MeV. We estimate the peak fluxes of the other 10 events in a similar way described by Park et al. (2015). As a result, we obtain 40 measurements of 18 SEPs by the multiple spacecraft.

For the information of flares and CMEs related to the 18 SEPs, we use the GOES flare list (http://solar-center.stanford.edu/SID/activities/PickFlare.html), the SOHO LASCO CME catalogue (http://cdaw.gsfc.nasa.gov/CME_list), and the SECCHI-A and B CME lists (http://secchi.nrl.navy.mil/cactus). To obtain 3D CME parameters, we use STEREO CME Analysis Tool (StereoCAT), which is provide by NASA CCMC (http://ccmc.gsfc.nasa.gov/analysis/stereo/). In the StereoCAT, the 3D CME parameters are measured by two coronagraphs out of three coronagraphs: SOHO/LASCO C3, STEREO-A, and B SECCHI COR2 images. We list the the mean values of 3D CME speeds and angular widths, which are obtained from running StereoCAT. Lee et al. (2015) estimated the errors of radial speed and angular width of StereoCAT using 44 halo CMEs from 2010 to 2011. They are about 7.6% and 9.7%, respectively.

The magnetic footpoints of the spacecraft are calculated by the simple Parker spiral field formula considering the solar wind speeds, which is given by $\varphi_0 = D\Omega/V_W + \varphi$, where φ_0 and φ represent the solar longitude and the longitude of a spacecraft, and D, Ω, and V_W represent the distance to the Sun, the Carrington period of 27.3 days, and solar wind speed, respectively. V_W is obtained from the ACE Solar Wind Electron Proton Alpha Monitor (SWEPAM: McComas et al. 1998) and the STEREO Plasma and Suprathermal Ion Composition (PLASTIC: Galvin et al. 2008) measurements. One main uncertainty comes from the determination of magnetic footpoints since the footpoints are affected by several physical conditions from Sun to the Earth. Lario et al. (2014) compared the footpoints obtained by three different models, Parker spiral field, MAS, and PFSS on the event of 2011 April 11, and found that the longitude differences among the models are within 20°.

Table 6. The properties of flares and CMEs that are associated with 18 SEP events. V_L is 2D CME speed and V_R is 3D CME speed. AW_L is 2D angular width and V_R is 3D angular width.

Flare[a]					CME[b]				
Date	Max	Class	Location	AR	Time	V_L ($km\,s^{-1}$)	V_R ($km\,s^{-1}$)	AW_L (°)	AW_R (°)
20100814	10:05	C4.4	N17W52	11099	10:12	1205	1152	360	110
20100818	05:48	C4.5	N17W91	11099	05:48	1471	1528	184	140
20110321	···	···	N22W132	···	02:24	1341	1493	360	136
20110607	06:41	M2.5	S21W64	11226	06:49	1255	1230	360	78
20110804	03:57	M9.3	N15W49	11261	04:12	1315	2025	360	134
20110809	08:05	X6.7	N17W83	11263	08:12	1610	1433	360	94
20110921	···	···	N15W120	···	22:12	1007	1148	255	108
20111126	07:10	C1.2	N08W49	11353	07:12	933	1068	360	124
20120127	18:37	X1.7	N27W71	11402	18:27	2508	3027	360	156
20120526	···	···	N15W120	···	20:57	1966	2121	360	110
20120614	14:35	M1.9	S17E14	11054	14:12	987	1126	360	98
20120723	···	···	S17W135	···	02:36	2003	2258	360	108
20120831	20:43	C8.4	S19E42	11564	20:12	1442	1628	360	116
20130315	06:58	M1.1	N11E12	11692	07:12	1063	1416	360	112
20130411	07:16	M6.5	N09E12	11719	07:24	861	1109	360	106
20130515	01:48	X1.2	N11E51	11748	01:48	1366	1667	360	130
20130522	13:22	M5	N15W70	11745	13:25	1466	1771	360	134
20130621	03:14	M2.9	S16E66	11777	03:12	1900	2097	207	158

4-2 Result

In the present study, we have examined characteristics of 18 SEP events from 2010 August to 2013 June using stereoscopic observation. For this, proton peak flux detected by SOHO and STEREO, 3D CME parameters (3D CME speed, 3D angular width, and θ_S), and 2D CME parameters (2D CME speed and angular width) are used. Major results from this study are summarized as follows. 1) We find that the dependence of SEPs on 3D CME speed (r=0.40) are similar to that of 2D CME speed (r=0.39) because the obtained radial speeds from StereoCat are not much different from the projected ones (Figure 7). 2) As shown in Figure 8, there is a weak tendency that the SEP peak flux increases with 3D angular width (r=0.33), while the 2D angular widths of all CMEs except for three events are 360°. 3) In the present study, SEP peak flux is strongly dependent on θ_S compared with CME speed and angular width. There is a noticeable anti-correlation (r=-0.62) between SPE peak flux and angular separation for 40 measurements (Figure 9). 4) All 17 measurements whose magnetic footpoints are located inside the CME angular widths, have SEP enhancements but about 40% of the measurements (14/37) whose footpoints are located outside, have no SEP enhancement. 5) Multiple spacecraft observations show that most strong SEP events are associated with very fast CMEs whose angular separations are closer to zero within the 3D angular widths (Figure 10). Bemporad & Mancuso (2011) showed that by SOHO/LASCO observation on 1999 June 11 event, the shock compression ratio (downstream/upstream plasma density) increases from the shock flanks to the shock center, which supporting strong SEP generation at the CME shock nose in the corona.

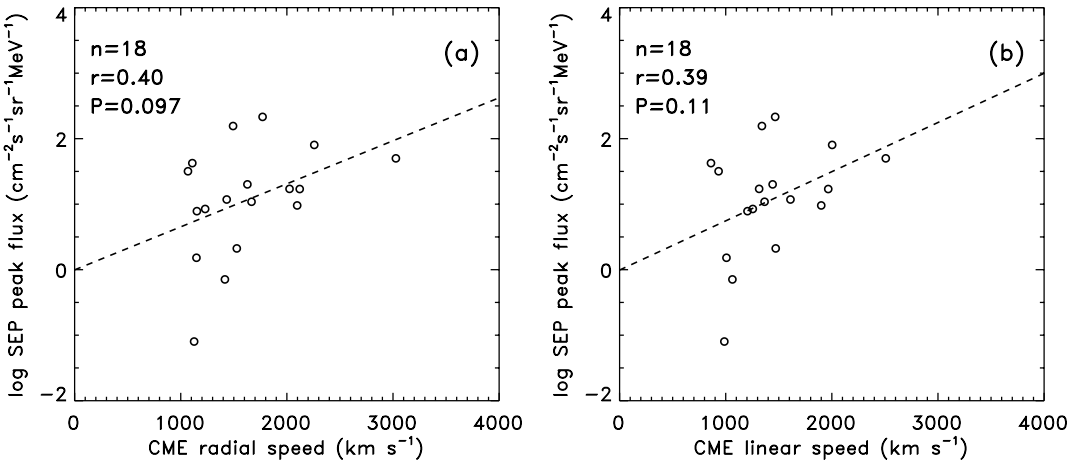

Figure 7. The relationship between SEP peak flux and (a) 3D CME speed as well as (b) 2D CME speed. The dashed line represents a linear square fit. In the figure, n, r, and p represent number of data, correlation coefficient, and p-value, respectively.

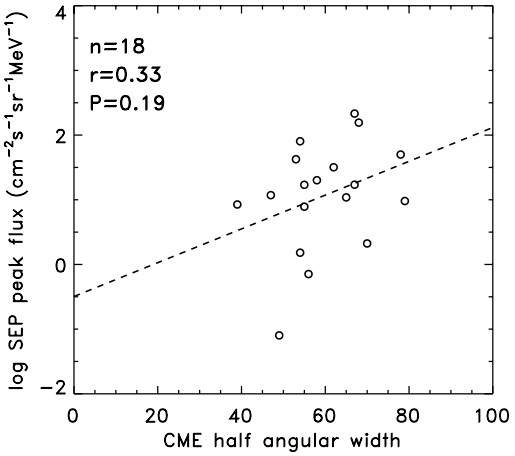

Figure 8. The relationship between SEP peak flux and 3D CME angular width.

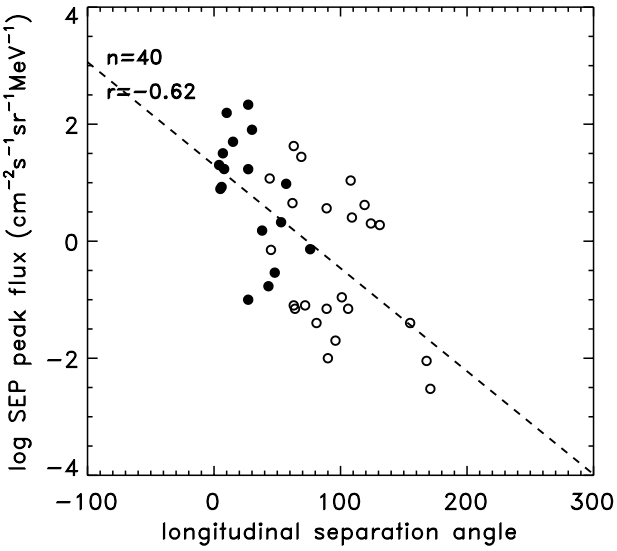

Figure 9. The relationship between the absolute value of longitudinal angular separation (|θS |) and the SEP peak flux. Filled circles represent that the magnetic footpoints of spacecraft are located inside the longitudinal boundaries of 3D angular width. Open circles represent that the magnetic footprints of spacecraft are located outside the longitudinal boundaries of 3D angular width.

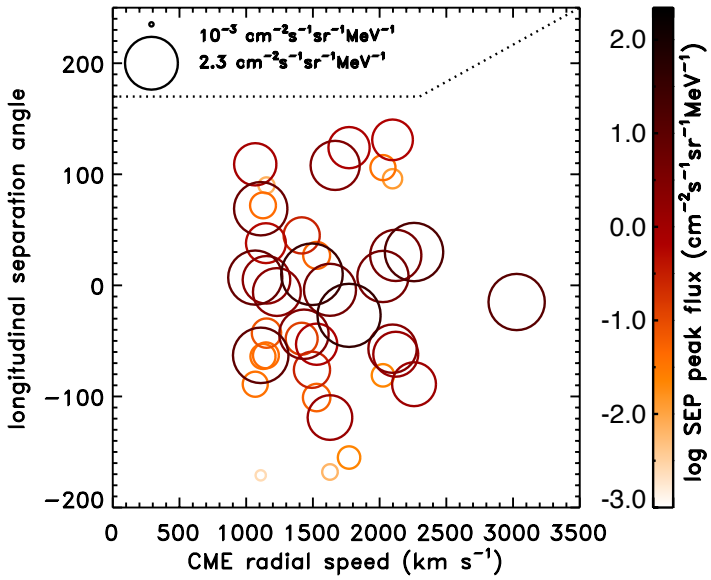

Figure 10. Proton peak flux as a function of 3D CME speed and longitudinal angular separation (θ_S). The red and green bar represent SEP peak fluxes associated with in-boundary and out-boundary of 3D angular widths, respectively.

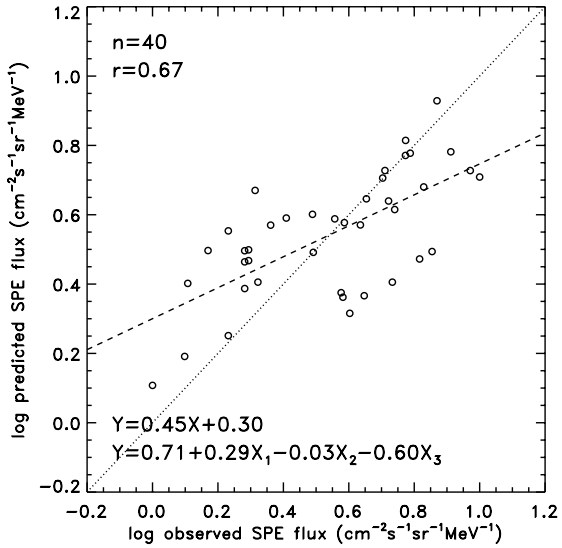

Figure 11. Relationship between the observed and the predicted SPE peak fluxes, which are estimated by the multiple regression method using 3D CME speed (X_1), 3D angular width (X_2), and longitudinal separation angle (X_3).

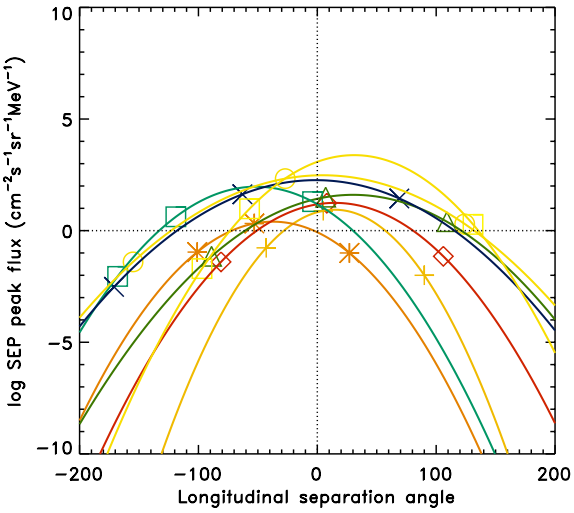

Figure 12. Least-square polynomial fits of the fluxes on 8 SEP events, which are observed SOHO, STEREO-A, and B. The symbols represent observed peak fluxes.

We use multiple regression method to examine the relations between 3D CME parameters (3D CME speed, 3D angular width, θ_S) and observed SEP peak fluxes. Figure 11 shows that the most importance parameter for SEP peak fluxes is separation angle. Figure 12 shows that 6-10 MeV proton peak fluxes decrease by one order of magnitude every 40-90°. The maximum peak fluxes are located near 0 separation angle.

The above results have shown that the proton peak fluxes are dependent on 3D CME parameters: radial speed, angular width, and longitudinal angular separation. In the case of CME-driven shocks, the Alfven Mach number, which indicates the strength of a shock, can be described by V_R/V_A where V_A is the Alfven speed. This equation implies that the faster the CME speed is, the stronger its associated shock is. The angular width of a CME seems to be associated with the volume of shock-forming regions. Thus we expect that the number of proton particles accelerated by the CME piston driven shocks have a tendency to increase with angular width. The angular separation is directly linked to the magnetic field connectivity of the spacecraft. Our results, for the first time, demonstrate that 3D CME physical parameters are very important for the generation of energetic proton particles in the corona.

5. Fe/O enhancement of solar energetic particles observed by multiple spacecraft (In preparation)

We study Fe/O enhancements of 16 solar energetic particles depending on current sheet effect (Table 7). There is a weak tendency that Fe/O enhancements are observed in multiple spacecraft where the magnetic footpoints of spacecraft are located in the same polarity of a solar source region. One of representative events is the event of 2010 August 18. The magnetic footpoints of Earth and STERE-A are connected to the same polarity of SEP solar source region (N17W91) and Fe/O enhancements are observed in the two spacecraft (Figure 13 and 14).

Table 7. Solar source of 16 solar energetic particles.

	Flare[a]					CME[b]		Radio[c]	
Date	Start	Max	Class	Location	AR	Time	V(kms^{-1})	type II	type III
20100814*	09:38	10:05	C4.4	N17W52	11099	$10:12^{L}$	1205^{L}	10:00	09:55
20100818*	04:45	05:48	C4.5	N17W91	11099	$05:24^{A}$	1250^{A}	06:05	05:30
20110307*	19:43	20:12	M3.7	N24W59	11164	$20:00^{L}$	2256^{L}	20:00	19:50
20110321*	···	···	···	N22W132	···	$02:24^{B}$	1562^{B}	02:20	02:20
20110804*	03:41	03:57	M9.3	N15W49	11261	$03:54^{A}$	1785^{A}	04:15	03:50
20110921*	···	···	···	N15W120	···	$22:12^{L}$	1007^{L}	···	21:40
20110922*	10:28	11:01	X1.4	N11E74	11302	$10:48^{L}$	1905^{L}	11:05	10:40
20111103*	···	···	···	N05E160	···	$22:54^{A}$	1136^{A}	22:35	22:15
20120123*	03:38	03:59	M8.7	N28W36	11402	$03:54^{B}$	1785^{B}	04:00	03:40
20120526	···	···	···	N15W120	11482	$20:57^{L}$	1966^{L}	20:50	20:45
20120718	···	···	···	N15W170	···	$06:24^{B}$	1041^{B}	06:15	05:55
20120723	···	···	···	S17W135	···	$02:36^{L}$	2003^{L}	02:30	02:10
20120831	19:45	20:43	C8.4	S19E42	11564	$20:12^{L}$	1442^{L}	20:00	19:50
20130315	05:46	06:58	M1.1	N11E12	11692	$07:12^{B}$	1136^{B}	07:00	06:40
20130411	06:55	07:16	M6.5	N09E12	11719	$07:24^{B}$	1388^{B}	07:10	07:00
20130513	01:53	02:17	X1.7	N08E89	11748	$02:12^{L}$	1302^{L}	02:20	02:05

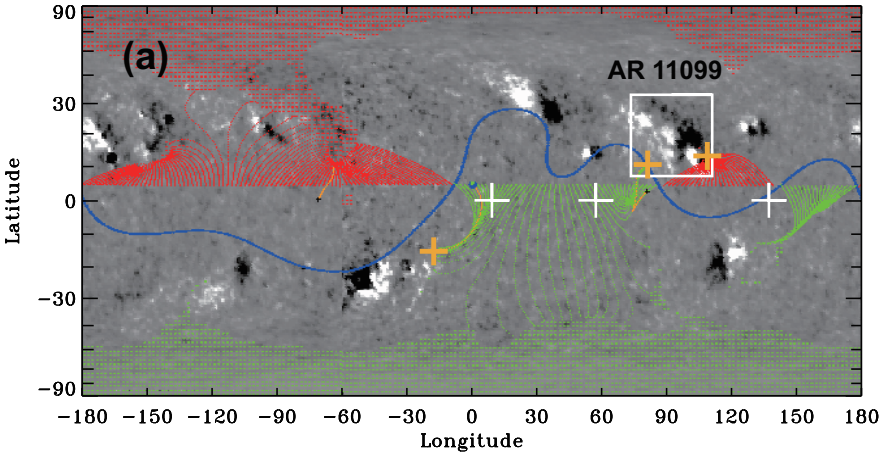

Figure 13. 2010 August 18 GONG synoptic magnetic field with PFSS ecliptic plane field lines traced back to their source. White crosses mark the longitudes of STB, Earth, and STA at 2.5R⊙. The photospheric footpoints of the connecting field lines are marked by orange crosses. Connecting footpoints are deduced by tracing the field lines from the white crosses to the Sun. Green/red indicates positive/negative open fields. The source region is enclosed by a white square.

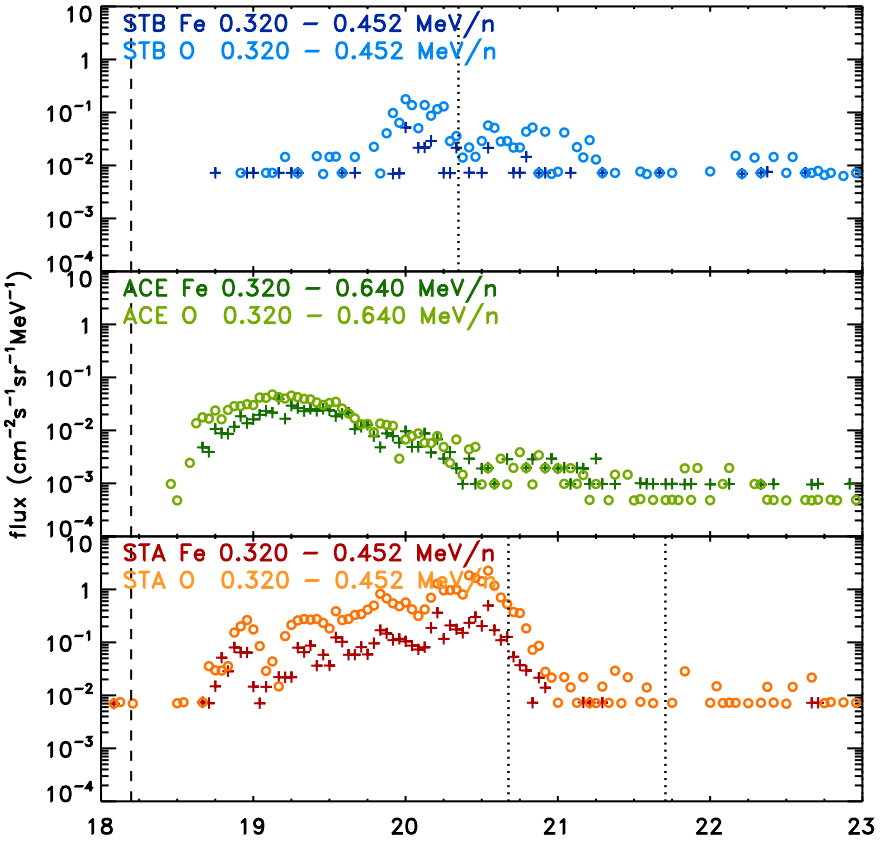

Figure 14. The SEP event of 2010 August 18

Figure 15 shows the relations between EUV wave speed and SEP peak. Same polarity case means the magnetic footpoint of spacecraft is same with the leading magnetic polarity of SEP source region and opposite polarity case means the magnetic footpoint of spacecraft is opposite with the leading magnetic polarity of SEP source. In the same polarity case, the correlation coefficient between EUV wave speed and SEP peak flux is a bit higher than those of all 16 events data set and the opposite case.

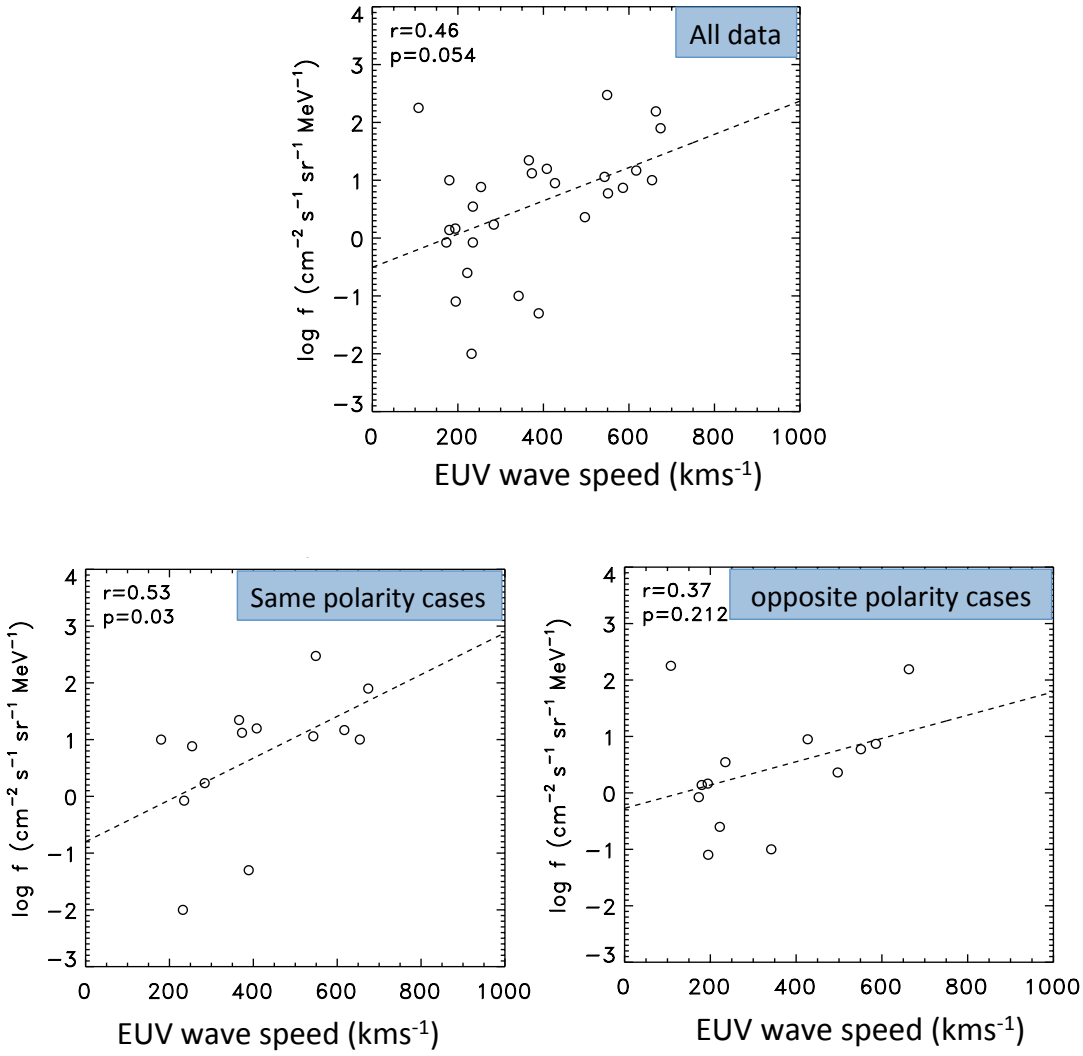

Figure 15. Relations between EUV wave speed and SEP peak flux. The top figure shows all 16 events. The bottom left figure is in the case where the magnetic footpoints are located in the same polarity of source region. The bottom right figure is in the case where the magnetic footpoints are located in the opposite polarity of source region.

Figure 16 shows the relations between separation angle and SEP peak fluxes depending on current sheet effect: same polarity and opposite polarity. Separation angle means angular distance between the SEP source region and the magnetic footpoint of spacecraft. SEP peak flux is more dependent on separation angle in the opposite polarity case (r = -0.6) than the same polarity case (-0.3).

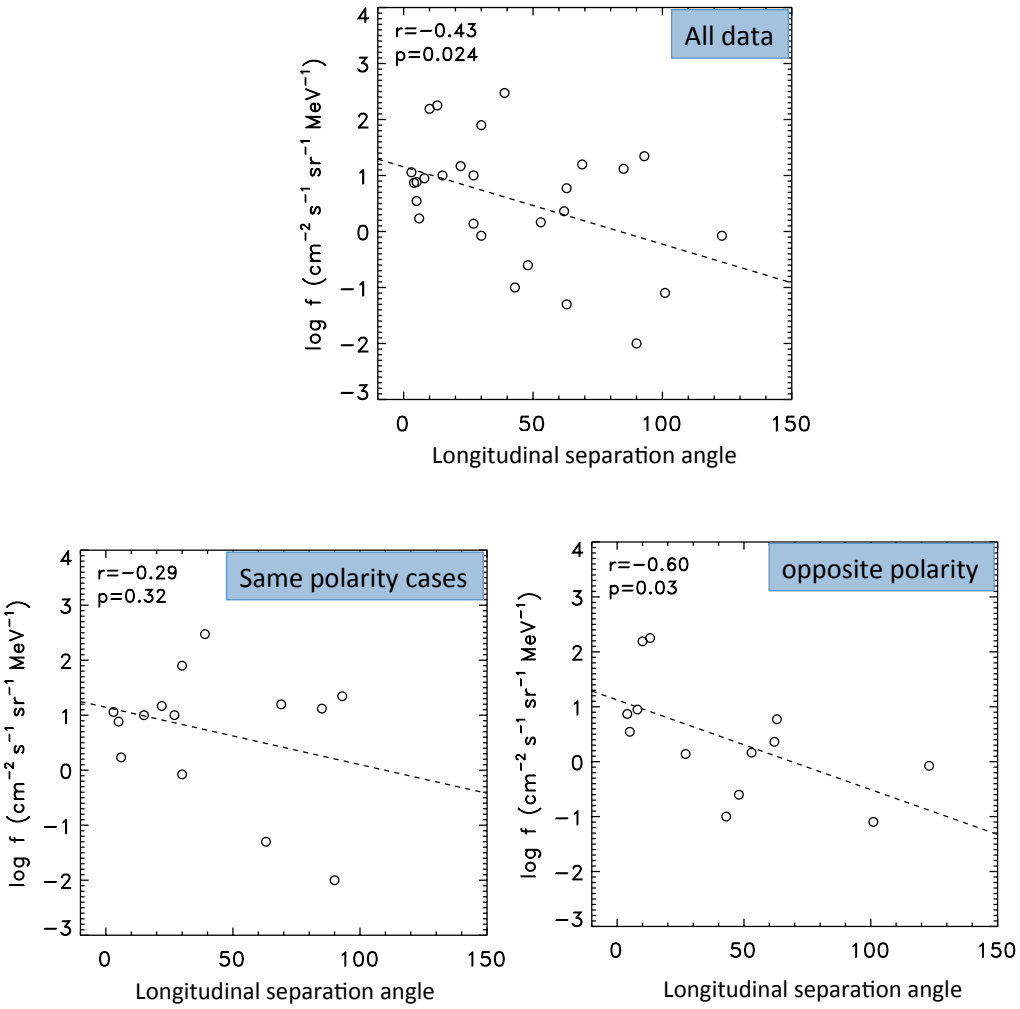

Figure 16. Relations between longitudinal separation angle and SEP peak flux. The top figure shows all 16 events. The bottom left figure is in the case where the magnetic footpoints are located in the same polarity of source region. The bottom right figure is in the case where the magnetic footpoints are located in the opposite polarity of source region.